

1  
2 **Evaluating the glacial-deglacial carbon respiration and ventilation**  
3 **change hypothesis as a mechanism for changing atmospheric CO<sub>2</sub>**

4  
5 **Lowell D. Stott<sup>1</sup>, Jun Shao<sup>1</sup>, Jimin Yu<sup>2</sup>, and Kathleen M. Harazin<sup>2</sup>**

6 **<sup>1</sup>Department of Earth Sciences, University of Southern California, 3651 Trousdale Pkwy,**  
7 **Los Angeles, CA 90089**

8 **<sup>2</sup>Research School of Earth Sciences, The Australian National University, Canberra, ACT**  
9 **2601, Australia**

10  
11 **Corresponding author: Lowell D. Stott (mailto: stott@usc.edu)**

12 **Key Points**

- 13     • **Highly-resolved proxy records of surface to deep water  $\delta^{13}\text{C}$  and  $\Delta^{14}\text{C}$  gradients from the**  
14 **Pacific are similar in the late Holocene and last glacial maximum.**
- 15     • **Model simulations of the prevailing hypothesis for enhanced respired carbon**  
16 **accumulation do not match observations of  $\delta^{13}\text{C}$ ,  $\Delta^{14}\text{C}$  and  $\epsilon^{14}\text{C}$  in the deep Pacific.**
- 17     • **Processes other than carbon respiration and ocean stratification must also be involved in**  
18 **explaining lower [O<sub>2</sub>] in the deep sea lower pCO<sub>2</sub> during the last glacial.**

19

## 20 **Abstract**

21 The prevailing hypothesis to explain pCO<sub>2</sub> rise at the last glacial termination calls upon enhanced  
22 ventilation of excess respired carbon that accumulated in the deep sea during the glacial. Recent  
23 studies argue lower [O<sub>2</sub>] in the glacial ocean is indicative of increased carbon respiration. The  
24 magnitude of [O<sub>2</sub>] depletion was 100-140 μmol/kg at the glacial maximum. Because respiration is  
25 coupled to δ<sup>13</sup>C of dissolved inorganic carbon (DIC), [O<sub>2</sub>] depletion of 100-140 μmol/kg from  
26 carbon respiration would lower deep water δ<sup>13</sup>C<sub>DIC</sub> by ~ 1‰ relative to surface water. Prolonged  
27 sequestration of respired carbon would also lower the amount of <sup>14</sup>C in the deep sea. We show  
28 that Pacific Deep Water δ<sup>13</sup>C<sub>DIC</sub> did not decrease relative to the surface ocean and Δ<sup>14</sup>C was only  
29 ~50‰ lower during the late glacial. Model simulations of the hypothesized ventilation change  
30 during deglaciation lead to large increases in δ<sup>13</sup>C<sub>DIC</sub>, Δ<sup>14</sup>C and ε<sup>14</sup>C that are not recorded in  
31 observations.

32

## 33 **Plain Language Summary**

34 The prevailing hypothesis to explain atmospheric CO<sub>2</sub> variability during glacial/interglacial  
35 cycles assumes atmospheric CO<sub>2</sub> was sequestered into the deep sea as respired metabolic carbon.  
36 Recent studies argue in support of this by suggesting lower oxygen concentrations in the deep  
37 Pacific during the glacial reflects increased oxidation of marine organic matter that promoted a  
38 larger accumulation of respired carbon. We show this interpretation is not validated by  
39 independent tests, including records of deep water δ<sup>13</sup>C and Δ<sup>14</sup>C.

## 40 **1 Introduction**

41 For over three decades efforts have been underway to identify the Earth System processes  
42 that modulate the concentration of atmospheric CO<sub>2</sub> on glacial/interglacial time scales. The  
43 prevailing hypothesis to explain the glacial/interglacial pCO<sub>2</sub> variability calls upon ocean-

44 stratification and reduced ventilation of deep waters during glaciations. In this scenario  
45 atmospheric CO<sub>2</sub> is drawn down by the marine biological pump and respired metabolic carbon  
46 accumulates in a deep ocean reservoir that remains isolated from the atmosphere. Much of the  
47 research to test this hypothesis has focused on the last glacial termination where detailed records  
48 from ocean and ice cores have documented the sequence of events surrounding the last glacial  
49 termination and the rise in atmospheric pCO<sub>2</sub> from 18.5 to 15ka (Clark et al., 2012). These  
50 events include the Heinrich 1 ice and meltwater advance across the North Atlantic that disrupted  
51 deep water convection and the distribution of heat (Boyle, 2000; Hodell et al., 2017; McManus et  
52 al., 2004; Seidov and Maslin, 2001). In the Southern Ocean, sea ice retreat and enhanced wind  
53 forcing during the Heinrich 1 interval may have increased Ekman upwelling and altered air-sea  
54 gas exchange (Anderson et al., 2009; Eggleston and Galbraith, 2018; Khatiwala et al., 2019;  
55 Menviel et al., 2018). The increased upwelling is thought to have enhanced deep water  
56 ventilation and release of excess respired carbon from the deep ocean to the atmosphere  
57 (Anderson et al., 2009; Menviel et al., 2017; Sigman and Boyle, 2000). At the same time, the  
58 strength and position of the southern Westerlies remains a difficult variable to robustly assess  
59 from proxy records (Kohfeld et al., 2013; Sime et al., 2013).

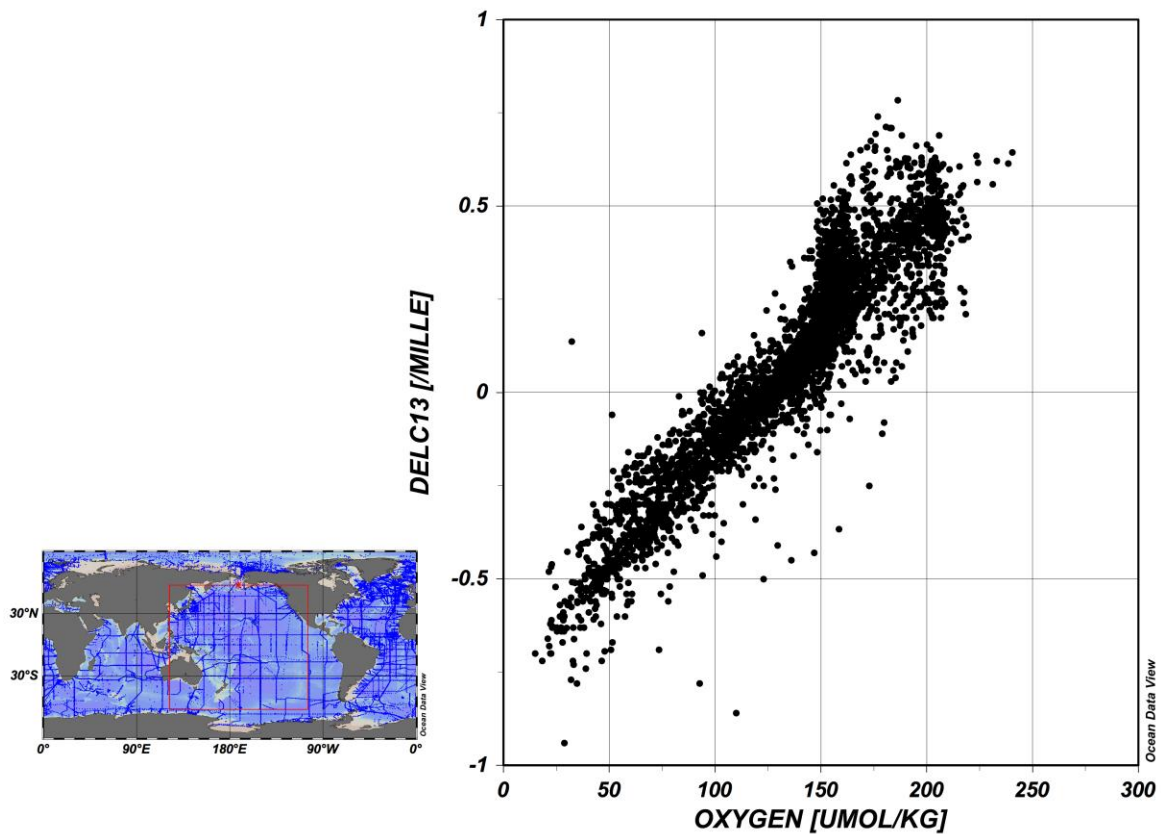
60         The respired carbon hypothesis calls upon increased accumulation and isolation of  
61 respired metabolic carbon in the deep sea due to greater ocean stratification and reduced  
62 ventilation rates relative to today (Adkins, 2013; Menviel et al., 2012; Menviel et al., 2017;  
63 Skinner et al., 2015). The hypothesis has recently been expanded to include accumulation of  
64 ‘old’ respired carbon throughout the deep Pacific (below 1500m) including the equatorial Pacific  
65 (Anderson et al., 2019; Jacobel et al., 2019). The evidence in support of an expanded respired-  
66 carbon reservoir comes from observations of lower dissolved oxygen concentrations in the

67 Pacific during the glacial. The lower oxygen levels during the glacial are attributed to the  
68 oxidation of organic carbon (Anderson et al., 2019; Jaccard and Galbraith, 2012; Jacobel et al.,  
69 2019), which would enhance the concentration of dissolved carbon. However, recent studies  
70 have found no evidence of enhanced productivity and export production in either the Eastern or  
71 Western Equatorial Pacific (Costa et al., 2016; Winckler et al., 2016), implying that if the  
72 respired carbon inventory increased, it must have been sourced from elsewhere. Such a scenario  
73 would require that additional respired carbon  $C_{org}$  and lower  $[O_2]$  be transported to the deep  
74 Pacific via a conduit from higher latitudes, specifically the Southern Ocean because productivity  
75 appears to have been reduced in the North Pacific (Jaccard et al., 2010). Early box-models (Knox  
76 and McElroy, 1984) simulated depleted  $[O_2]$  in the Southern Ocean and have been validated by  
77 proxy data (Jaccard et al., 2016; Lu et al., 2016).

78 An issue that complicates the inference of enhanced respired carbon from proxies of  $[O_2]$   
79 is the potential influence of air-sea disequilibrium on preformed  $[O_2]$  in the deep water source  
80 region (Eggleston and Galbraith, 2018). In particular, expanded sea ice may have had a strong  
81 influence on air-sea exchange of  $CO_2$ , and perhaps also on  $O_2$  (Khaliwala et al., 2019). Large  
82 uncertainties exist, especially since the equilibration time for  $O_2$  is a magnitude smaller than that  
83 of  $CO_2$ . However, modern studies suggest a diminishing and proportional relationship between  
84 air-sea exchange and the fraction of sea ice up to ~90%, with seasonal and annual variability in  
85 Southern Ocean preformed  $O_2$  at least partly attributable to sea ice and its indirect effects on  
86 biology (Bushinsky et al., 2017). Because zones of the South Ocean exhibit  $[O_2]$  undersaturation  
87 during austral winter, expanded sea ice and shorter summer melting seasons are likely to have  
88 reduced air-sea exchange and lowered preformed  $[O_2]$  in the glacial deep Pacific. For this reason,  
89 lower  $[O_2]$  values in the deep Pacific during the last glacial cannot be directly converted to

90 estimates of carbon respiration without an independent form of validation. Here we use a  
 91 separate proxy to assess how much of the oxygen concentration change in Pacific deep water can  
 92 be attributed to metabolic carbon oxidation.

93 If oxygen depletion in the deep Pacific was solely the result of carbon respiration, there  
 94 would have been an accompanying shift in deep water  $^{13}\text{C}/^{12}\text{C}$  (referred to as  $\delta^{13}\text{C}$  in ‰ relative  
 95 to the VPDB standard). This is because photosynthetic carbon is depleted in  $^{13}\text{C}$  by  
 96 approximately 20‰ relative to dissolved carbon in surface waters. As photosynthetic carbon is  
 97 oxidized in the subsurface,  $^{12}\text{C}$  is added back to the pool of DIC, lowering its  $\delta^{13}\text{C}$ . This  
 98 relationship is illustrated in Figure 1 where the  $\delta^{13}\text{C}$  of DIC is plotted versus dissolved  $[\text{O}_2]$  in  
 99 the deep Pacific. In the modern ocean a decrease in  $[\text{O}_2]$  of ~100-140  $\mu\text{mol}/\text{kg}$  is accompanied  
 100 by a lowering of  $\delta^{13}\text{C}$  by nearly 1‰ (Figure 1).



101 **Figure 1.** Plot of  $\delta^{13}\text{C}$  of DIC vs dissolved  $\text{O}_2$  from the GLODAP database of sites in the Pacific.  
 102

103 Over time deep waters lose [O<sub>2</sub>] and acquire lower δ<sup>13</sup>C values as oxidized metabolic carbon is  
104 added.

105 If the waters in the deep Pacific lost 100 to 140 μmol/kg of [O<sub>2</sub>] during the last glacial  
106 maximum due entirely to metabolic carbon oxidation it would be reflected in the δ<sup>13</sup>C of calcitic  
107 benthic foraminifera relative to surface water δ<sup>13</sup>C as recorded by planktic foraminifera. The  
108 calcite of the surface-dwelling planktic foraminifera *Globigerinoides ruber* s.s. records changes  
109 in the δ<sup>13</sup>C of western equatorial surface waters in contact with the atmosphere (Kawahata, 2005;  
110 Lin et al., 2004; Numberger et al., 2009) with a species-specific offset of 0.9‰ for specimens  
111 between 250-350 μm (Spero et al., 2003). Preindustrial δ<sup>13</sup>C<sub>DIC</sub> values of the western equatorial  
112 tropical surface waters would have been between 1.9-2.3‰ (Eide et al., 2017), values that are  
113 simulated well in current climate models (Menviel et al., 2015). The average δ<sup>13</sup>C of late  
114 Holocene *G. ruber* in the western equatorial Pacific is 1.3‰ (1σ=0.3‰) (Figure 2). With a  
115 species-specific offset of 0.9 the late Holocene *G. ruber* are recording an average late Holocene  
116 δ<sup>13</sup>C<sub>DIC</sub> value of 2.1‰ ±0.3‰, very close to the modern, preindustrial value. The epibenthic  
117 foraminifer *Cibicidoides mundulus* records the δ<sup>13</sup>C of dissolved inorganic carbon of Pacific  
118 Deep Water, with minor influences from CO<sub>3</sub><sup>=</sup> and pressure (Schmittner et al., 2017). The δ<sup>13</sup>C  
119 offset between late Holocene *G. ruber* and *C. mundulus* is ~1.3‰ and therefore is very close to  
120 the modern (pre-Industrial) surface to deep water δ<sup>13</sup>C gradient. We use the δ<sup>13</sup>C of fossil *G.*  
121 *ruber* and *C. mundulus* from a sediment core collected at 2114m in the western equatorial Pacific  
122 to reconstruct how the surface to Pacific Deep Water δ<sup>13</sup>C gradient has varied in time and  
123 evaluate whether the gradient was larger during the late glacial relative to the Holocene as the  
124 carbon respiration hypothesis predicts. Sediment core MD98-2181 was collected within the core  
125 of Pacific Deep Water, which is the oldest and among the most oxygen depleted waters in the

126 deep North Pacific today. This water mass would have carried the oldest, most oxygen deficient  
127 and most carbon-rich waters southward toward the Southern Ocean during the deglaciation.

128 The prevailing hypothesis also predicts that as excess respired carbon accumulated in a  
129 more stratified and less ventilated glacial ocean the  $^{14}\text{C}/^{12}\text{C}$  ( $\Delta^{14}\text{C}_{\text{DIC}}$ ) would have decreased  
130 relative to the surface ocean. Then, during the deglaciation both  $\Delta^{14}\text{C}_{\text{DIC}}$  and  $\delta^{13}\text{C}_{\text{DIC}}$  would have  
131 increased as older,  $\text{O}_2$ -poor deep waters were replaced by younger, better ventilated waters with  
132 higher  $\delta^{13}\text{C}_{\text{DIC}}$  (Menviel et al., 2018). We test this prevailing hypothesis by comparing new and  
133 existing data from the deep Pacific with the predictions and with an Earth System Model  
134 (LOVECLIM) simulation that depicts the timing and magnitude of  $\delta^{13}\text{C}$  and  $\Delta^{14}\text{C}$  response to the  
135 hypothesized changes in deep water ventilation.

## 136 **2 Materials and Methods**

### 137 **2.1 $\delta^{13}\text{C}$ and $\Delta^{14}\text{C}$ proxies**

138 The MD98-2181 core was collected from the margin of Mindanao where the flux of  
139 terrigenous sediments to the sea floor is high and consequently the temporal resolution of  
140 individual samples from this core is also very high. Typical sediment accumulation rates are  
141 between 60 and 80cm/ky (Stott et al., 2007; Stott et al., 2004). The planktic foraminifera  $\delta^{13}\text{C}$   
142 values (*Globigerinoides ruber s.s.*) are not affected by upwelling of subsurface waters and thus  
143 reflect the  $\delta^{13}\text{C}$  of surface water DIC. The  $\delta^{13}\text{C}$  of the benthic foraminifera (*Cibicidoides*  
144 *mundulus*) record the history of Pacific Deep Water  $\delta^{13}\text{C}$  DIC. Culturing studies have shown that  
145 this benthic foraminifer may migrate from the sediment water interface into the shallow most  
146 sediments briefly if disturbed but rapidly (within 24 hours) returns to the sediment water  
147 interface (Wollenburg et al., 2018). It appears therefore this species spends most of its life at the  
148 sediment water interface. After the MD98-2181 core was split, discrete samples were extracted

149 at 1 to 2-centimeter intervals. The samples were dried at 40°C and then disaggregated in a  
150 buffered solution of water and sodium hexametaphosphate. The disaggregated sediment was then  
151 washed over at >63 $\mu$ m screen to remove the finer material and then dried again. Planktic and  
152 benthic foraminifera from each sample were picked under a microscope. For stable isotope  
153 measurements the planktic species *Globigerinoides ruber* (white) was picked from the greater  
154 than 250 $\mu$ m fraction. The benthic species *Cibicidoides mundulus* (s.l.) was picked from the  
155 >180 $\mu$ m size fraction. The picked specimens were gently cracked open between glass slides,  
156 transferred to small centrifuge tubes and sonicated in buffered DI water for several seconds to  
157 remove fine debris (via syringe) from the calcite. After drying the calcite was loaded into vials  
158 for stable isotope analysis on a Micromass Instruments Isoprime Isotope Ratio Mass  
159 Spectrometer located at the University of Southern California following standard procedures in  
160 which a sample of CO<sub>2</sub> from the calcite is compared to a reference gas calibrated to the NBS  
161 PDB standard for both  $\delta^{13}\text{C}$  and  $\delta^{18}\text{O}$ . Average precision of the USC inhouse calcite standard  
162 (Ultiss) averaged <0.1‰ for  $\delta^{13}\text{C}$ . Note, the  $\delta^{13}\text{C}$  data from core MD98-2181 has not been  
163 published previously. Only the oxygen isotope data from this core have been published  
164 previously (Stott et al., 2007).

165 For radiocarbon measurements, different species of planktic and benthic foraminifera  
166 were picked, depending on the interval and the abundances of species. Specimens were cleaned  
167 in the same fashion as those for stable isotope measurements. The analyses were conducted at the  
168 Woods Hole Oceanographic Institution Accelerator Mass Spectrometry (AMS) Laboratory and  
169 at the Keck Carbon Cycle AMS Laboratory at the University of California Irvine. In samples  
170 with enough *C. mundulus* (s.l.), *Cibicidoides wuellerstorffii* and *Uvigerina* for single species  
171 measurements, we analyzed more than one species to assess reproducibility. Typical



172 reproducibility of both benthic and planktic samples were within 300-500 years. There were  
173 intervals of the core where abundances were too low to obtain a measurement from a single  
174 species. In these cases, mixed species were used. There is also a portion of the core between  
175 935cm and 1100cm that is disturbed and samples from this interval are not included in the study.  
176 Estimates of  $\Delta^{14}\text{C}$  are based on the following equation:

$$177 \quad \Delta^{14}\text{C} = (\text{Fm} * e^{\lambda/(\text{calendar age})-1}) * 1000\text{‰}$$

178 Where Fm is the fraction of modern,  $\lambda = 1/8,267$  is the decay constant for  $^{14}\text{C}$  and a 5,730 year  
179 half-life (Stuiver and Polach, 1977). The uncertainties include the compounded analytical  
180 uncertainty of Fm and calendar ages. Calendar ages for the MD98-2181 samples were obtained  
181 by converting planktic  $^{14}\text{C}$  ages to a calendar age using BChroncalibrate ages (Haslett and  
182 Parnell, 2008) with the Marine 20 calibration curve and a constant reservoir age. The surface  
183 reservoir age offset ( $\Delta\text{R}$ ) in the western tropical Pacific today is 0-50 years (Clark et al., 2006;  
184 Southon, 2002). There is no indication that the reservoir age of surface waters in the western  
185 tropical Pacific varied significantly during the past 22 thousand years. Thus, we applied a  
186 reservoir age correction ( $\Delta\text{R}=0$ ) to each planktic  $^{14}\text{C}$  age from the MD98-2181 core  
187 (supplemental Table 1). The metric  $\epsilon^{14}\text{C} = ((\Delta^{14}\text{C}_{\text{benthic}}/1000+1)/(\Delta^{14}\text{C}_{\text{atm}}/1000+1)-1) * 1000$  is  
188 used to characterize the  $^{14}\text{C}$  disequilibrium between the contemporaneous deep ocean and the  
189 atmosphere (Soulet et al., 2016).

190 The  $1\sigma$  uncertainties of  $\Delta^{14}\text{C}$  and  $\epsilon^{14}\text{C}$  are derived through a Monte-Carlo approach that fully  
191 propagates the uncertainties of  $^{14}\text{C}$  measurements, calibrated calendar ages, atmospheric  $\Delta^{14}\text{C}$   
192 values from the IntCal20 curve. These data are archived on PANGEA.

### 193 **3 Results and Discussion**

194 The deep Pacific [ $\text{O}_2$ ] is estimated to have been  $\sim 100\text{-}140\mu\text{mol/kg}$  lower during the  
195 glacial (Anderson et al., 2019). If that lowering of  $\text{O}_2$  was due entirely to metabolic carbon  
196 oxidation (Anderson et al., 2019) it would have lowered deep Pacific  $\delta^{13}\text{C}_{\text{DIC}}$  by  $1.0\text{‰}$  beyond  
197 the global mean ocean  $\delta^{13}\text{C}$  shift that is recorded by planktic foraminifera that inhabited the  
198 surface ocean where carbon respiration would not influence the  $\delta^{13}\text{C}$  of DIC (Figure 1).

#### 199 **3.1 The Carbon Oxidation Hypothesis versus Pacific $\delta^{13}\text{C}$ Records During the Glacial**

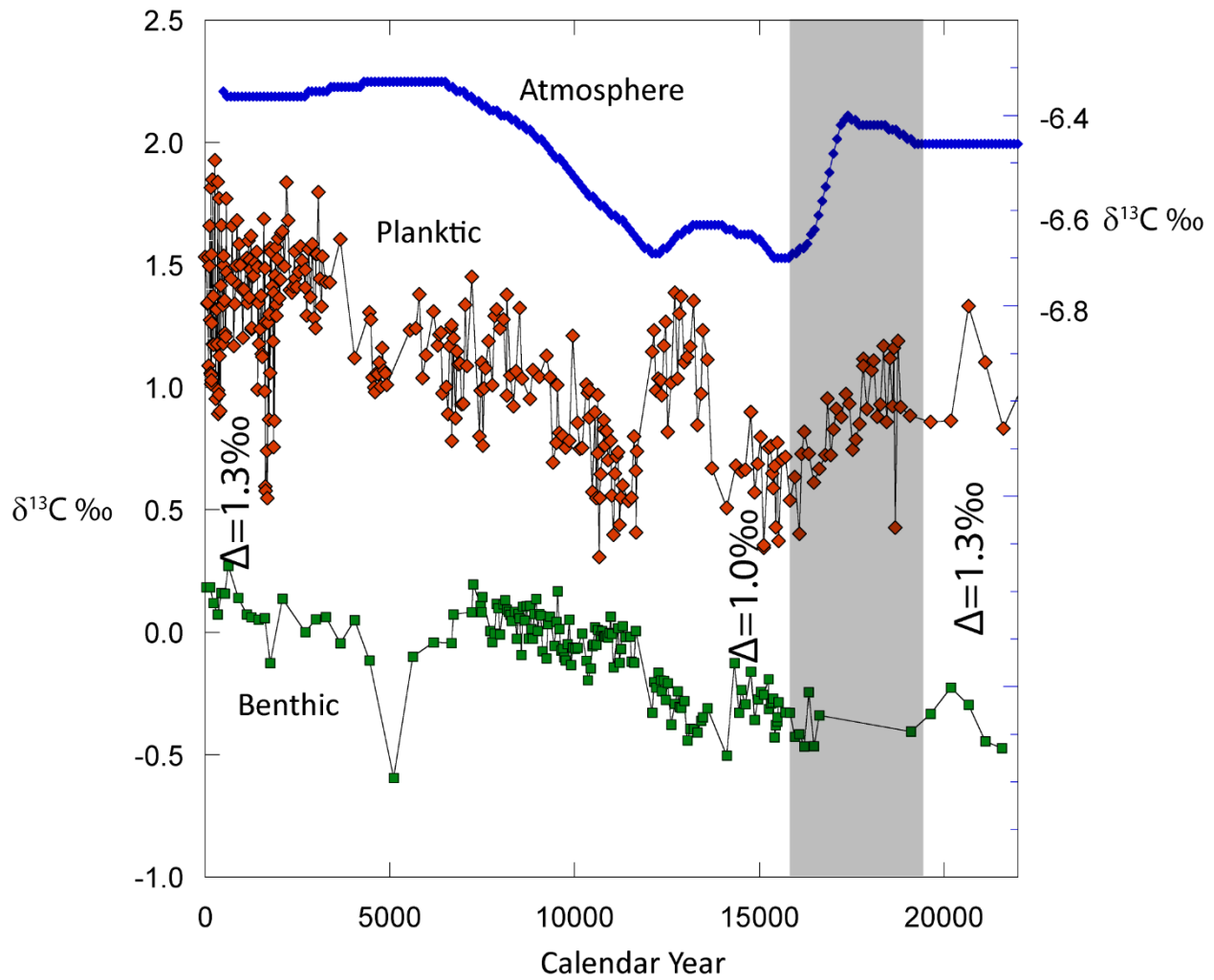
200 In Figure 2 we illustrate the  $\delta^{13}\text{C}$  values of surface-dwelling planktic and bottom-dwelling  
201 benthic foraminifera from core MD98-2181. We find that the  $\delta^{13}\text{C}$  offset between the surface  
202 ocean (planktic values) and Pacific Deep Water (benthic values) was  $\sim 1.3\text{‰}$  in the late Holocene  
203 as it is in the modern ocean and was also  $1.3\text{‰}$  in the late glacial. Both the Holocene and the late  
204 glacial offsets between the tropical surface ocean and deep Pacific were therefore very close to  
205 the modern ocean offset. There is no evidence that Pacific Deep Water  $\delta^{13}\text{C}$  values were  $2.3\text{‰}$   
206 lower than planktic values during the late glacial (the modern offset of  $1.3\text{‰}$  plus the  $1\text{‰}$  shift  
207 due to the oxidation of additional marine organic carbon) as required by the carbon oxidation  
208 hypothesis (Anderson et al., 2019).

#### 209 **3.2 Deep Pacific $\delta^{13}\text{C}$ and $\Delta^{14}\text{C}$ Data Do Not Support a Significant Increase in Ventilation 210 Rate at the Glacial Termination**

211 There are relatively few high-resolution benthic  $\delta^{13}\text{C}$  records from the deep Pacific that  
212 span the last glacial termination. The results from MD98-2181 are shown in Figure 3 together

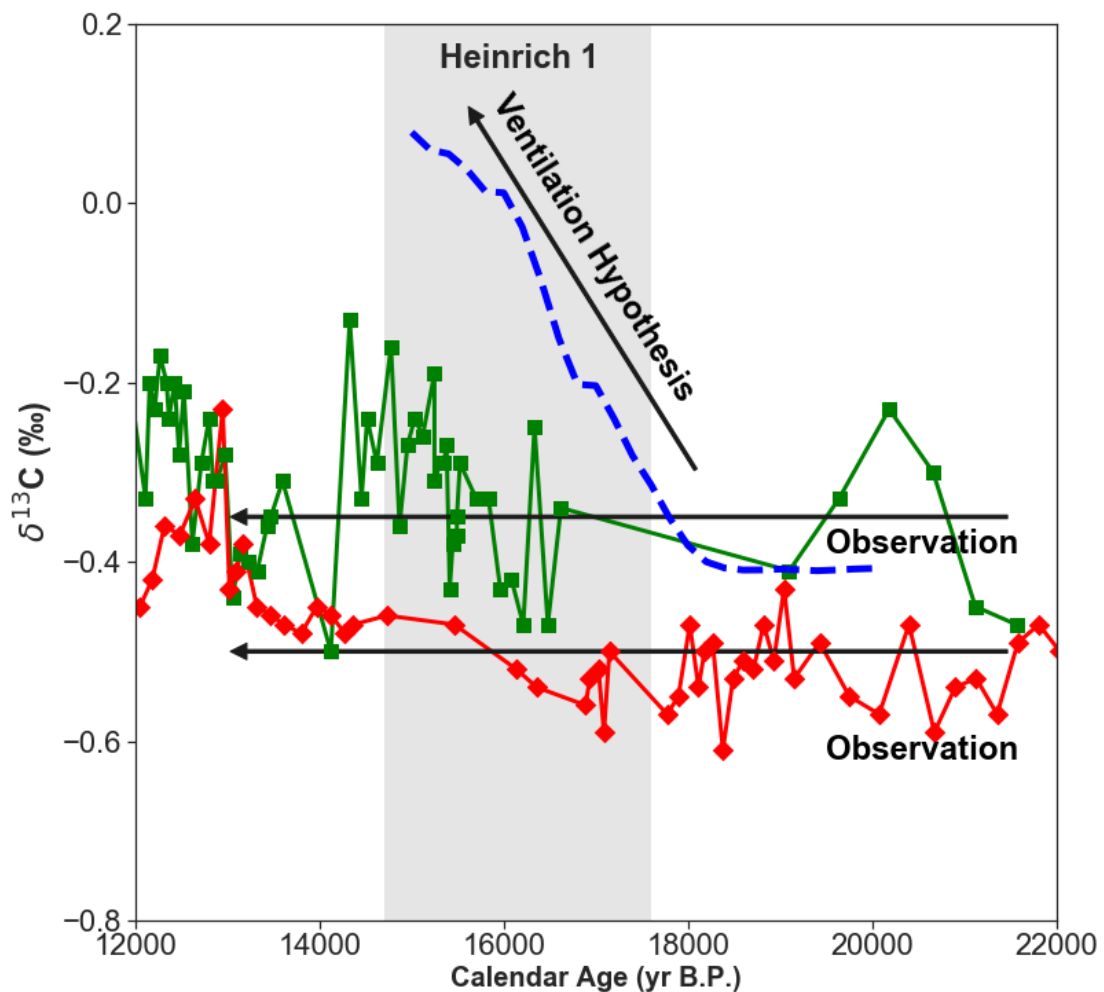
213 with another well-resolved record from the deep North Pacific (Lund and Mix, 1998; Lund et al.,  
214 2011). In neither of these records is there evidence that deep Pacific  $\delta^{13}\text{C}$  values increased during  
215 the Heinrich 1 interval as predicted by the ocean ventilation hypothesis (Meniel et al., 2018)  
216 (Figure 2). It is possible that the LOVECLIM simulation overestimates the amount of ventilation  
217 in the deep Pacific and therefore overpredicts the magnitude of  $\delta^{13}\text{C}$  increase during the early  
218 deglaciation. However, the fact that both sites do not record anomalously low glacial  $\delta^{13}\text{C}$  values  
219 and do not record an increase in  $\delta^{13}\text{C}$  during the early deglacial is not consistent with the  
220 prevailing hypothesis that calls for enhanced carbon oxidation to explain the lower glacial  $[\text{O}_2]$   
221 and increased  $[\text{O}_2]$  during the deglaciation.

222



223  
224  
225  
226  
227  
228

Figure 2. The record of atmospheric  $\delta^{13}\text{C}$  ( $\text{CO}_2$ ) (Schmitt et al., 2012), planktic (*G. ruber*)  $\delta^{13}\text{C}$  and benthic (*C. mundulus*)  $\delta^{13}\text{C}$  from core MD98-2181 from the western tropical Pacific. All values are plotted relative to the VPDB standard. Located at 2114m water depth, the core is bathed today by Pacific Deep Water.



229

230 Figure 3. Benthic  $\delta^{13}\text{C}$  (Obs) from deep Pacific cores MD98-2181 (green, this study) and  
 231 W8709A-13PC (red) (Lund and Mix, 1998; Lund et al., 2011) and the LOVECLIM simulated  
 232 Deep Pacific  $\delta^{13}\text{C}_{\text{DIC}}$  response to enhanced ventilation (blue) (Menviel et al., 2018).  
 233

234 Like  $\delta^{13}\text{C}_{\text{DIC}}$ , the  $\Delta^{14}\text{C}_{\text{DIC}}$  values of Pacific Deep Water starts as a preformed value  
 235 acquired in the Southern Ocean source region where AABW and UCDW waters are subducted to  
 236 abyssal depths. Pacific Deep Water is the product of aging of these waters as they flow towards  
 237 the North Pacific and gradually upwell (Talley, 2013). The  $\Delta^{14}\text{C}_{\text{DIC}}$  values decrease as waters

238 age during northward transit through the ocean and are transformed into Pacific Deep Water that  
239 then returns to the Southern Ocean (Key et al., 2004). Today, Antarctic surface water  $\Delta^{14}\text{C}$   
240 values are close to -100‰. Circumpolar deep waters are  $\sim$ -150‰. Pacific Deep Water has the  
241 lowest  $\Delta^{14}\text{C}$  in the ocean of  $\sim$ -200‰ (Figure S1), reflecting the roughly 1400 year residence  
242 time of deep water in the Pacific (Khatiwala et al., 2012; Primeau and Holzer, 2006). The  
243 western tropical Pacific surface water  $\Delta^{14}\text{C}$  values are 0-50‰. The offset between tropical surface  
244 water and Pacific Deep Water today is therefore,  $\sim$  200-250‰ (Figure S1).

245         The radiocarbon content of deep and surface water is recorded in the calcite tests of  
246 bottom and surface-dwelling foraminifera. Using the radiocarbon decay constant and calendar  
247 ages for each interval of a sediment core the  $^{14}\text{C}$  age of planktic and benthic foraminifers are  
248 converted to radiocarbon activity ( $\Delta^{14}\text{C}$ ) (Methods). The surface (planktic) to deep water  
249 (benthic)  $\Delta^{14}\text{C}$  offset in the late Holocene and in the late glacial was 150‰, very close to the  
250 modern offset (Figures S1 and S2). Therefore, there is no evidence that there was a much larger  
251 offset in the late glacial period that would be indicative of a longer residence time of Pacific  
252 Deep Water. These findings are supported by other, lower resolution results from the deep  
253 Pacific that do not document lower  $^{14}\text{C}$  content during the last glacial maxima (Broecker et al.,  
254 2008; Broecker et al., 2004). Importantly, we show that high resolution  $\Delta^{14}\text{C}$  values at MD98-  
255 2181 in the deep Pacific does not record a large increase during the early deglaciation as the  
256 prevailing hypothesis predicts (Menviel et al., 2018). The offset remains the same for 5 thousand  
257 years after the beginning of deglaciation as atmospheric  $\text{pCO}_2$  rose by 35-40ppm.

258         For the purpose of using benthic  $\Delta^{14}\text{C}$  and atmospheric  $\Delta^{14}\text{C}$  offset to trace ventilation,  
259  $\epsilon^{14}\text{C}$  is perhaps a more accurate metric, where more negative values reflect a larger gradient  
260 between the deep and surface (see Method).  $\epsilon^{14}\text{C}$  at the MD98-2181 site is  $\sim$ 250‰ during the

261 LGM and ~200‰ during Holocene (Figure S2 lower panel). The 50‰ glacial-interglacial offset  
262 is consistent with changes in benthic-atmospheric  $\Delta^{14}\text{C}$  (Figure S2 upper panel). There are small  
263 increases occur during the Heinrich 1 and Younger Dryas time intervals (Figure S2). These  
264 shorter term features are also seen in other high resolution records from the North Pacific (Lund  
265 et al. 2013).

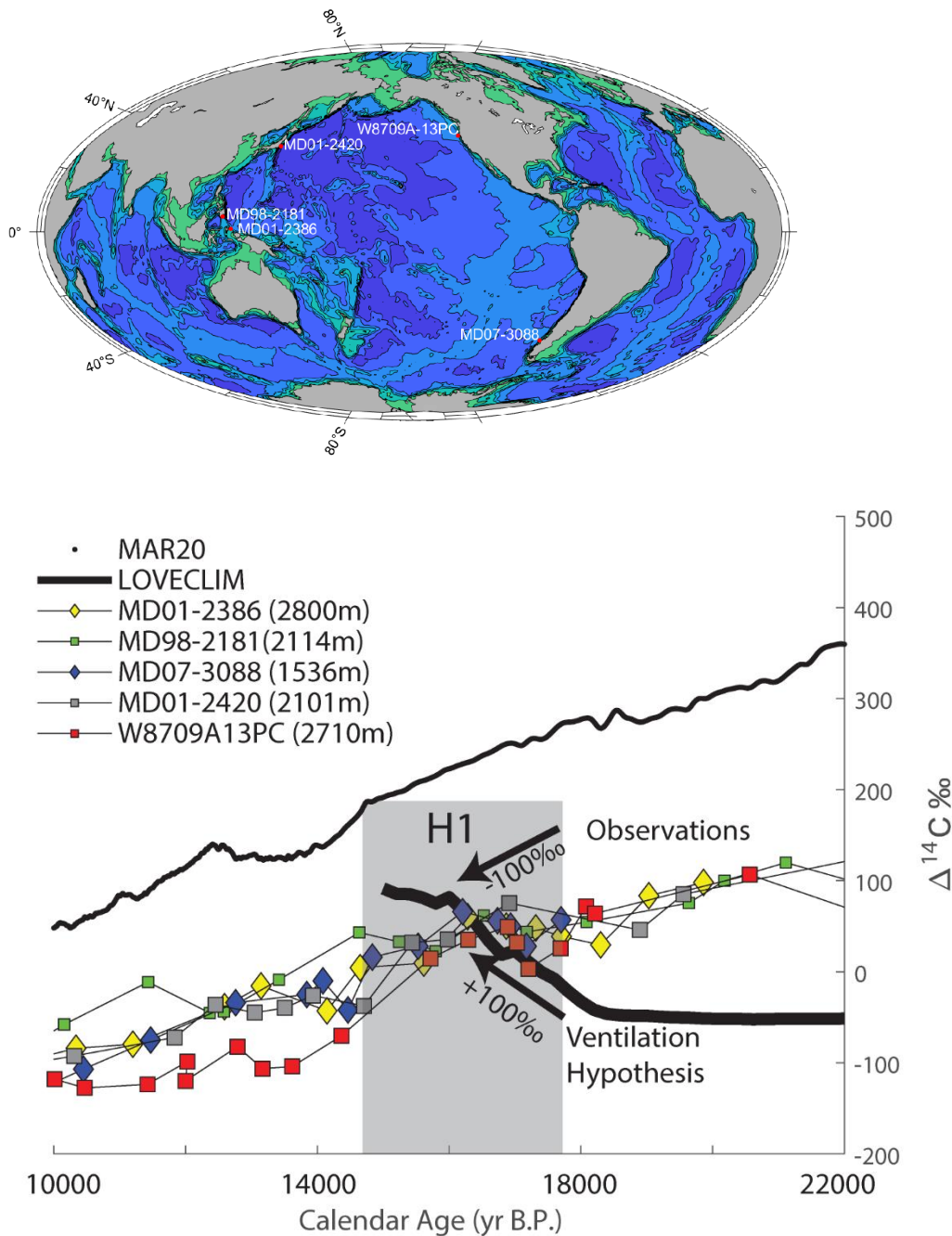
266 In Figure 4 the benthic  $\Delta^{14}\text{C}$  record for MD98-2181 is plotted together with four  
267 previously published benthic  $\Delta^{14}\text{C}$  records from deep water sites in both the north and south  
268 Pacific. These records are plotted with the simulated values from the Earth System Model  
269 (LOVECLIM) for the deep Pacific  $\Delta^{14}\text{C}$  in response to increased deep water ventilation at the  
270 onset of deglaciation (Menviel et al., 2018). In each of the observational records, spanning water  
271 depths between ~1500 and 2800m, there is a ~100‰ decrease in  $\Delta^{14}\text{C}$  between 17.5 and 14.5ka  
272 whereas the model simulates a 100‰ increase over this time interval. The observational records  
273 of deep water  $\Delta^{14}\text{C}$  document a decline in both the North and South Pacific as atmospheric  
274  $\text{pCO}_2$  was rising. This is in direct conflict with results from the LOVECLIM experiment that  
275 simulates the deep Pacific response to enhanced ventilation. Considering that the absolute values  
276 of atmospheric  $\Delta^{14}\text{C}$  during the last glacial termination (i.e. from IntCal20) are different from the  
277 simulated atmospheric  $\Delta^{14}\text{C}$  in LOVECLIM,  $\epsilon^{14}\text{C}$  for the observational data and the model data  
278 are also calculated to allow a direct comparison of  $^{14}\text{C}$ -based ventilation state from the data and  
279 from the model (Figure S2). The simulated deep Pacific  $\epsilon^{14}\text{C}$  shows a rapid 150‰ increase,  
280 while the observations only record a 50‰ increase. This contrast in  $\epsilon^{14}\text{C}$  clearly indicates the  
281 model overestimates the degree of enhanced ventilation during the early deglaciation.

282

283

284

285



286

287

288

289

290

291

Figure 4. Upper Panel, Deep Pacific core locations. Lower Panel Benthic  $\Delta^{14}\text{C}$  from the deep Pacific cores. Lower Panel, MARINE20 (global surface ocean)  $\Delta^{14}\text{C}$  (Heaton et al., 2020). The solid black line is the simulated deep Pacific (130E-130W, 0-50N, 2000-3000m)  $\Delta^{14}\text{C}$  response to enhanced ventilation during the deglaciation using LOVECLIM (Meniel et al., 2018). Core MD98-2181 data is from this study. Raw  $^{14}\text{C}$  ages from Core MD01-2386 (Broecker et al.,



292 2008); MD07-3088 (Siani et al., 2013); MD01-2420 (Okazaki, 2012); W8709A-13PC (Lund,  
293 2013).

#### 294 **4 Conclusions**

295 The observational data now available from the deep Pacific Ocean spanning the last  
296 25kys do not support the prevailing hypothesis that calls upon significantly reduced deep water  
297 ventilation rate and enhanced accumulation of respired carbon. The small (50‰) decrease in  
298  $\epsilon^{14}\text{C}$  may reflect some reduction in ventilation rate during the LGM but not to the extent that it  
299 affected the amount of respired carbon that accumulated as there is no indication that the  $\delta^{13}\text{C}$  of  
300 Pacific Deep Water was lower as would have occurred if the reduced  $[\text{O}_2]$  was due entirely to  
301 carbon respiration. We suggest a more likely explanation for lower deep-water oxygen  
302 concentrations during the glacial was reduced  $\text{O}_2$  ocean-atmosphere equilibration in the source  
303 regions where deep waters formed, warranting further investigation into past variability of  
304 preformed  $\text{O}_2$  of deep source waters.

#### 305 **Acknowledgments, Samples, and Data**

306 We are indebted to Laurie Menviel for sharing her LOVECLIM model simulations.

307 We also greatly appreciate the support of John Southon for the  $^{14}\text{C}$  measurements used in this  
308 study. We also acknowledge the financial support of the National Science Foundation. The stable  
309 isotope and  $^{14}\text{C}$  age data from MD98-2181 are available on PANGEA.

310

311

#### 312 **References**

- 313 Adkins, J. F. (2013), The role of deep ocean circulation in setting glacial climates, *Paleoceanography*, 28(3),  
314 539-561, doi: 10.1002/palo.20046.
- 315 Anderson, R. F., S. Ali, L. I. Bradtmiller, S. H. H. Nielsen, M. Q. Fleisher, B. E. Anderson, and L. H. Burckle  
316 (2009), Wind-Driven Upwelling in the Southern Ocean and the Deglacial Rise in Atmospheric  $\text{CO}_2$ ,  
317 *Science*, 323(5920), 1443-1448, doi: 10.1126/science.1167441.
- 318 Anderson, R. F., J. P. Sachs, M. Q. Fleisher, K. A. Allen, J. Yu, A. Koutavas, and S. L. Jaccard (2019), Deep-Sea  
319 Oxygen Depletion and Ocean Carbon Sequestration During the Last Ice Age, *Global Biogeochemical*  
320 *Cycles*, 33(3), 301-317, doi: 10.1029/2018gb006049.

- 321 Boyle, E. A. (2000), Is ocean thermohaline circulation linked to abrupt stadial/interstadial transitions?, *Quaternary*  
 322 *Science Reviews*, 19(1-5), 255-272.
- 323 Broecker, W., E. Clark, and S. Barker (2008), Near constancy of the Pacific Ocean surface to mid-depth  
 324 radiocarbon-age difference over the last 20 kyr, *Earth and Planetary Science Letters*, 274(3-4), 322-326,  
 325 doi: <http://dx.doi.org/10.1016/j.epsl.2008.07.035>.
- 326 Broecker, W., S. Barker, E. Clark, I. Hajdas, G. Bonani, and L. Stott (2004), Ventilation of the Glacial Deep Pacific  
 327 Ocean, *Science*, 306, 1169-1172.
- 328 Bushinsky, S. M., A. R. Gray, K. S. Johnson, and J. L. Sarmiento (2017), Oxygen in the Southern Ocean From Argo  
 329 Floats: Determination of Processes Driving Air-Sea Fluxes, *Journal of Geophysical Research: Oceans*,  
 330 122(11), 8661-8682, doi: 10.1002/2017jc012923.
- 331 Clark, G., A. Anderson, and D. Wright (2006), Human Colonization of the Palau Islands, Western Micronesia, *The*  
 332 *Journal of Island and Coastal Archaeology*, 1(2), 215-232, doi: 10.1080/15564890600831705.
- 333 Clark, P. U., et al. (2012), Global climate evolution during the last deglaciation, *Proceedings of the National*  
 334 *Academy of Sciences*, 109(19), E1134-E1142, doi: 10.1073/pnas.1116619109.
- 335 Costa, K. M., J. F. McManus, R. F. Anderson, H. Ren, D. M. Sigman, G. Winckler, M. Q. Fleisher, F. Marcantonio,  
 336 and A. C. Ravelo (2016), No iron fertilization in the equatorial Pacific Ocean during the last ice age,  
 337 *Nature*, 529(7587), 519-522, doi: 10.1038/nature16453.
- 338 Eggleston, S., and E. D. Galbraith (2018), The devil's in the disequilibrium: multi-component analysis of dissolved  
 339 carbon and oxygen changes under a broad range of forcings in a general circulation model, *Biogeosciences*,  
 340 15(12), 3761-3777, doi: 10.5194/bg-15-3761-2018.
- 341 Eide, M., A. Olsen, U. S. Ninnemann, and T. Eldevik (2017), A global estimate of the full oceanic 13C Suess effect  
 342 since the preindustrial, *Global Biogeochemical Cycles*, 31(3), 492-514, doi: 10.1002/2016gb005472.
- 343 Haslett, J., and A. Parnell (2008), A simple monotone process with application to radiocarbon - dated depth  
 344 chronologies, *Journal of the Royal Statistical Society: Series C (Applied Statistics)*, 57(4), 399-418, doi:  
 345 <https://doi.org/10.1111/j.1467-9876.2008.00623.x>.
- 346 Heaton, T. J., et al. (2020), Marine20—The Marine Radiocarbon Age Calibration Curve (0–55,000 cal BP),  
 347 *Radiocarbon*, 62(4), 779-820, doi: 10.1017/RDC.2020.68.
- 348 Hodell, D. A., et al. (2017), Anatomy of Heinrich Layer 1 and its role in the last deglaciation, *Paleoceanography*,  
 349 32(3), 284-303, doi: 10.1002/2016pa003028.
- 350 Jaccard, S. L., and E. D. Galbraith (2012), Large climate-driven changes of oceanic oxygen concentrations during  
 351 the last deglaciation, *Nature Geosci*, 5(2), 151-156, doi:  
 352 <http://www.nature.com/ngeo/journal/v5/n2/abs/ngeo1352.html#supplementary-information>.
- 353 Jaccard, S. L., E. D. Galbraith, D. M. Sigman, and G. H. Haug (2010), A pervasive link between Antarctic ice core  
 354 and subarctic Pacific sediment records over the past 800kyrs, *Quaternary Science Reviews*, 29(1), 206-212,  
 355 doi: <https://doi.org/10.1016/j.quascirev.2009.10.007>.
- 356 Jaccard, S. L., E. D. Galbraith, A. Martínez-García, and R. F. Anderson (2016), Covariation of deep Southern Ocean  
 357 oxygenation and atmospheric CO2 through the last ice age, *Nature*, 530(7589), 207-210, doi:  
 358 10.1038/nature16514.
- 359 Jacobel, A. W., R. F. Anderson, S. L. Jaccard, J. F. McManus, F. J. Pavia, and G. Winckler (2019), Deep Pacific  
 360 storage of respired carbon during the last ice age: Perspectives from bottom water oxygen reconstructions,  
 361 *Quaternary Science Reviews*, 106065, doi: <https://doi.org/10.1016/j.quascirev.2019.106065>.
- 362 Kawahata, H. (2005), Stable isotopic composition of two morphotypes of *Globigerinoides ruber* (white) in the  
 363 subtropical gyre in the North Pacific, *Paleontological Research*, 9(1), 27-35.
- 364 Key, R. M., A. Kozyr, C. L. Sabine, K. Lee, R. Wanninkhof, J. L. Bullister, R. A. Feely, F. J. Millero, C. Mordy,  
 365 and T.-H. Peng (2004), A global ocean carbon climatology: Results from Global Data Analysis Project  
 366 (GLODAP), *Global Biogeochemical Cycles*, 18(GB4031), doi:10.1029/2004GB002247, doi:  
 367 doi:10.1029/2004GB002247.
- 368 Khatiwala, S., F. Primeau, and M. Holzer (2012), Ventilation of the deep ocean constrained with tracer observations  
 369 and implications for radiocarbon estimates of ideal mean age, *Earth and Planetary Science Letters*, 325-  
 370 326, 116-125, doi: <https://doi.org/10.1016/j.epsl.2012.01.038>.
- 371 Khatiwala, S., A. Schmittner, and J. Muglia (2019), Air-sea disequilibrium enhances ocean carbon storage during  
 372 glacial periods, *Science Advances*, 5(6), eaaw4981, doi: 10.1126/sciadv.aaw4981.
- 373 Knox, F., and M. McElroy (1984), Changes in atmospheric CO<sub>2</sub>: influence of marine biota at high latitude, *Journal*  
 374 *of Geophysical Research*, 89, 4629-4637.

- 375 Kohfeld, K. E., R. M. Graham, A. M. de Boer, L. C. Sime, E. W. Wolff, C. Le Quéré, and L. Bopp (2013), Southern  
 376 Hemisphere westerly wind changes during the Last Glacial Maximum: paleo-data synthesis, *Quaternary*  
 377 *Science Reviews*, 68, 76-95, doi: <https://doi.org/10.1016/j.quascirev.2013.01.017>.
- 378 Lin, H.-L., W.-C. Wang, and G.-W. Hung (2004), Seasonal variation of planktonic foraminiferal isotopic  
 379 composition from sediment traps in the South China Sea, *Marine Micropaleontology*, 53(3), 447-460, doi:  
 380 <https://doi.org/10.1016/j.marmicro.2004.08.004>.
- 381 Lu, Z., B. A. A. Hoogakker, C.-D. Hillenbrand, X. Zhou, E. Thomas, K. M. Gutchess, W. Lu, L. Jones, and R. E. M.  
 382 Rickaby (2016), Oxygen depletion recorded in upper waters of the glacial Southern Ocean, *Nature*  
 383 *Communications*, 7, 11146, doi: 10.1038/ncomms11146.
- 384 Lund, D. C. (2013), Deep Pacific ventilation ages during the last deglaciation: Evaluating the influence of diffusive  
 385 mixing and source region reservoir age, *Earth and Planetary Science Letters*, 381, 52-62, doi:  
 386 <https://doi.org/10.1016/j.epsl.2013.08.032>.
- 387 Lund, D. C., and A. C. Mix (1998), Millennial-scale deep water oscillations: Reflections of the North Atlantic in the  
 388 deep Pacific from 10 to 60 ka, *Paleoceanography*, 13(1), 10-19, doi: 10.1029/97PA02984.
- 389 Lund, D. C., A. C. Mix, and J. Southon (2011), Increased ventilation age of the deep northeast Pacific Ocean during  
 390 the last deglaciation, *Nat Geosci*, 4(11), 771-774, doi: <https://doi.org/10.1038/ngeo1272>.
- 391 McManus, J. F., R. Francois, J. M. Gherardi, L. D. Keigwin, and S. Brown-Leger (2004), Collapse and rapid  
 392 resumption of Atlantic meridional circulation linked to deglacial climate changes, *Nature*, 428(6985), 834-  
 393 837.
- 394 Menviel, L., F. Joos, and S. P. Ritz (2012), Simulating atmospheric CO<sub>2</sub>, <sup>13</sup>C and the marine carbon cycle during the  
 395 Last Glacial-Interglacial cycle: possible role for a deepening of the mean remineralization depth and an  
 396 increase in the oceanic nutrient inventory, *Quaternary Science Reviews*, 56(0), 46-68, doi:  
 397 <http://dx.doi.org/10.1016/j.quascirev.2012.09.012>.
- 398 Menviel, L., A. Mouchet, K. J. Meissner, F. Joos, and M. H. England (2015), Impact of oceanic circulation changes  
 399 on atmospheric δ<sup>13</sup>C<sub>CO2</sub>, *Global Biogeochemical Cycles*, 29(11), 1944-1961, doi: 10.1002/2015gb005207.
- 400 Menviel, L., J. Yu, F. Joos, A. Mouchet, K. J. Meissner, and M. H. England (2017), Poorly ventilated deep ocean at  
 401 the Last Glacial Maximum inferred from carbon isotopes: A data-model comparison study,  
 402 *Paleoceanography*, 32(1), 2-17, doi: 10.1002/2016pa003024.
- 403 Menviel, L., P. Spence, J. Yu, M. A. Chamberlain, R. J. Matear, K. J. Meissner, and M. H. England (2018),  
 404 Southern Hemisphere westerlies as a driver of the early deglacial atmospheric CO<sub>2</sub> rise, *Nature*  
 405 *Communications*, 9(1), 2503, doi: 10.1038/s41467-018-04876-4.
- 406 Numberger, L., C. Hemleben, R. Hoffmann, A. Mackensen, H. Schulz, J.-M. Wunderlich, and M. Kucera (2009),  
 407 Habitats, abundance patterns and isotopic signals of morphotypes of the planktonic foraminifer  
 408 *Globigerinoides ruber* (d'Orbigny) in the eastern Mediterranean Sea since the Marine Isotopic Stage 12,  
 409 *Marine Micropaleontology*, 73(1), 90-104, doi: <https://doi.org/10.1016/j.marmicro.2009.07.004>.
- 410 Okazaki, Y., Sagawa, T., Asahi, H., Horikawa, K., and Onodera, J (2012), Ventilation changes in the western North  
 411 Pacific since the last glacial period., *Climate of the Past*, 8, 17-24, doi: 10.5194/cp-8-17-2012.
- 412 Primeau, F. W., and M. Holzer (2006), The Ocean's Memory of the Atmosphere: Residence-Time and Ventilation-  
 413 Rate Distributions of Water Masses, *Journal of Physical Oceanography*, 36(7), 1439-1456, doi:  
 414 10.1175/JPO2919.1.
- 415 Schmitt, J., et al. (2012), Carbon Isotope Constraints on the Deglacial CO<sub>2</sub> Rise from Ice Cores, *Science*, 336(6082),  
 416 711-714, doi: 10.1126/science.1217161.
- 417 Schmittner, A., et al. (2017), Calibration of the carbon isotope composition (δ<sup>13</sup>C) of benthic foraminifera,  
 418 *Paleoceanography*, 32(6), 512-530, doi: 10.1002/2016pa003072.
- 419 Seidov, D., and M. Maslin (2001), Atlantic Ocean heat piracy and the bipolar climate see-saw during Heinrich and  
 420 Dansgaard-Oeschger events, *Journal of Quaternary Science*, 16(4), 321-328.
- 421 Siani, G., E. Michel, R. De Pol-Holz, T. DeVries, F. Lamy, M. Carel, G. Isguder, F. Dewilde, and A. Lourantou  
 422 (2013), Carbon isotope records reveal precise timing of enhanced Southern Ocean upwelling during the last  
 423 deglaciation, *Nat Commun*, 4, doi: 10.1038/ncomms3758.
- 424 Sigman, D. M., and E. A. Boyle (2000), Glacial/interglacial variations in atmospheric carbon dioxide, *Nature*, 407,  
 425 859-869.
- 426 Sime, L. C., K. E. Kohfeld, C. Le Quéré, E. W. Wolff, A. M. de Boer, R. M. Graham, and L. Bopp (2013), Southern  
 427 Hemisphere westerly wind changes during the Last Glacial Maximum: model-data comparison, *Quaternary*  
 428 *Science Reviews*, 64, 104-120, doi: <https://doi.org/10.1016/j.quascirev.2012.12.008>.

- 429 Skinner, L., I. N. McCave, L. Carter, S. Fallon, A. E. Scrivner, and F. Primeau (2015), Reduced ventilation and  
430 enhanced magnitude of the deep Pacific carbon pool during the last glacial period, *Earth and Planetary*  
431 *Science Letters*, 411(0), 45-52, doi: <http://dx.doi.org/10.1016/j.epsl.2014.11.024>.
- 432 Soulet, G., L. C. Skinner, S. R. Beaupré, and V. Galy (2016), A Note on Reporting of Reservoir 14C Disequilibria  
433 and Age Offsets, *Radiocarbon*, 58(1), 205-211, doi: 10.1017/RDC.2015.22.
- 434 Southon, J., Kashgarian, M, Fontugne, M, Metivier, B, and Yim, W W-S, (2002), Marine reservoir corrections for  
435 the Indian Ocean and Southeast Asia., *Radiocarbon*, 44, 67-180.
- 436 Spero, H. J., K. M. Mielke, E. M. Kalve, D. W. Lea, and D. K. Pak (2003), Multispecies approach to reconstructing  
437 eastern equatorial Pacific thermocline hydrography during the past 360 kyr, *Paleoceanography*, 18(1), doi:  
438 1022
- 439 Artn 1022.
- 440 Stott, L., A. Timmermann, and R. Thunell (2007), Southern hemisphere and deep-sea warming led deglacial  
441 atmospheric CO<sub>2</sub> rise and tropical warming, *Science*, 318(5849), 435-438.
- 442 Stott, L., K. Cannariato, R. Thunell, G. H. Haug, A. Koutavas, and S. Lund (2004), Decline of surface temperature  
443 and salinity in the western tropical Pacific Ocean in the Holocene epoch, *Nature*, 431, 56-59.
- 444 Stuiver, M., and H. A. Polach (1977), Discussion Reporting of <sup>14</sup>C Data, *Radiocarbon*, 19(3), 355-363, doi:  
445 10.1017/S0033822200003672.
- 446 Talley, L. D. (2013), Closure of the Global Overturning Circulation Through the Indian, Pacific, and Southern  
447 Oceans. Schematics and Transports, *Oceanography*, 26(1), 80-97.
- 448 Winckler, G., R. F. Anderson, S. L. Jaccard, and F. Marcantonio (2016), Ocean dynamics, not dust, have controlled  
449 equatorial Pacific productivity over the past 500,000 years, *Proceedings of the National Academy of*  
450 *Sciences*, 113(22), 6119-6124, doi: 10.1073/pnas.1600616113.
- 451 Wollenburg, J. E., Z. M. C. Zittier, and J. Bijma (2018), Insight into deep-sea life – Cibicidoides pachyderma  
452 substrate and pH-dependent behaviour following disturbance, *Deep Sea Research Part I: Oceanographic*  
453 *Research Papers*, 138, 34-45, doi: <https://doi.org/10.1016/j.dsr.2018.07.006>.

454

455

456

457

458

459

460

461

462

463

464

465

466

467

468

469

470

471

472

473



474

475

[GRL]

476

Supporting Information for

477

478

Evaluating the glacial-deglacial carbon respiration and ventilation

479

change hypothesis as a mechanism for changing atmospheric CO<sub>2</sub>

480

**Lowell D. Stott<sup>1</sup>, Jun Shao<sup>1</sup>, Jimin Yu<sup>2</sup>, and Kathleen M. Harazin<sup>2</sup>**

481

**<sup>1</sup>Department of Earth Sciences, University of Southern California, 3651 Trousdale Pkwy,  
Los Angeles, CA 90089**

482

483

**<sup>2</sup>Research School of Earth Sciences, The Australian National University, Canberra, ACT  
2601, Australia**

484

485

486

487

**Contents of this file**

488

489

Figures S1 to S2

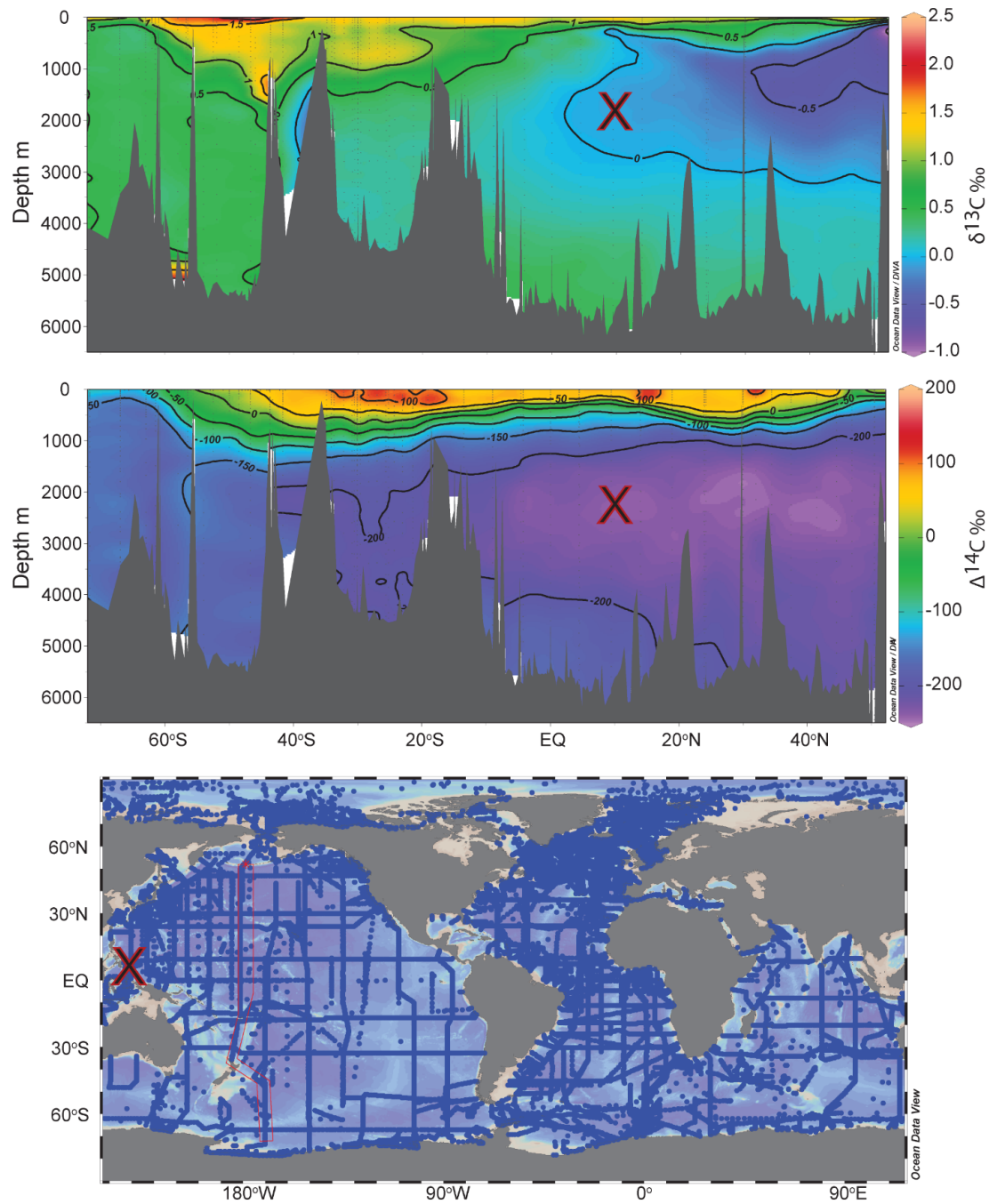
490

491

**Introduction**

492

The supplemental figures referred to in the manuscript.

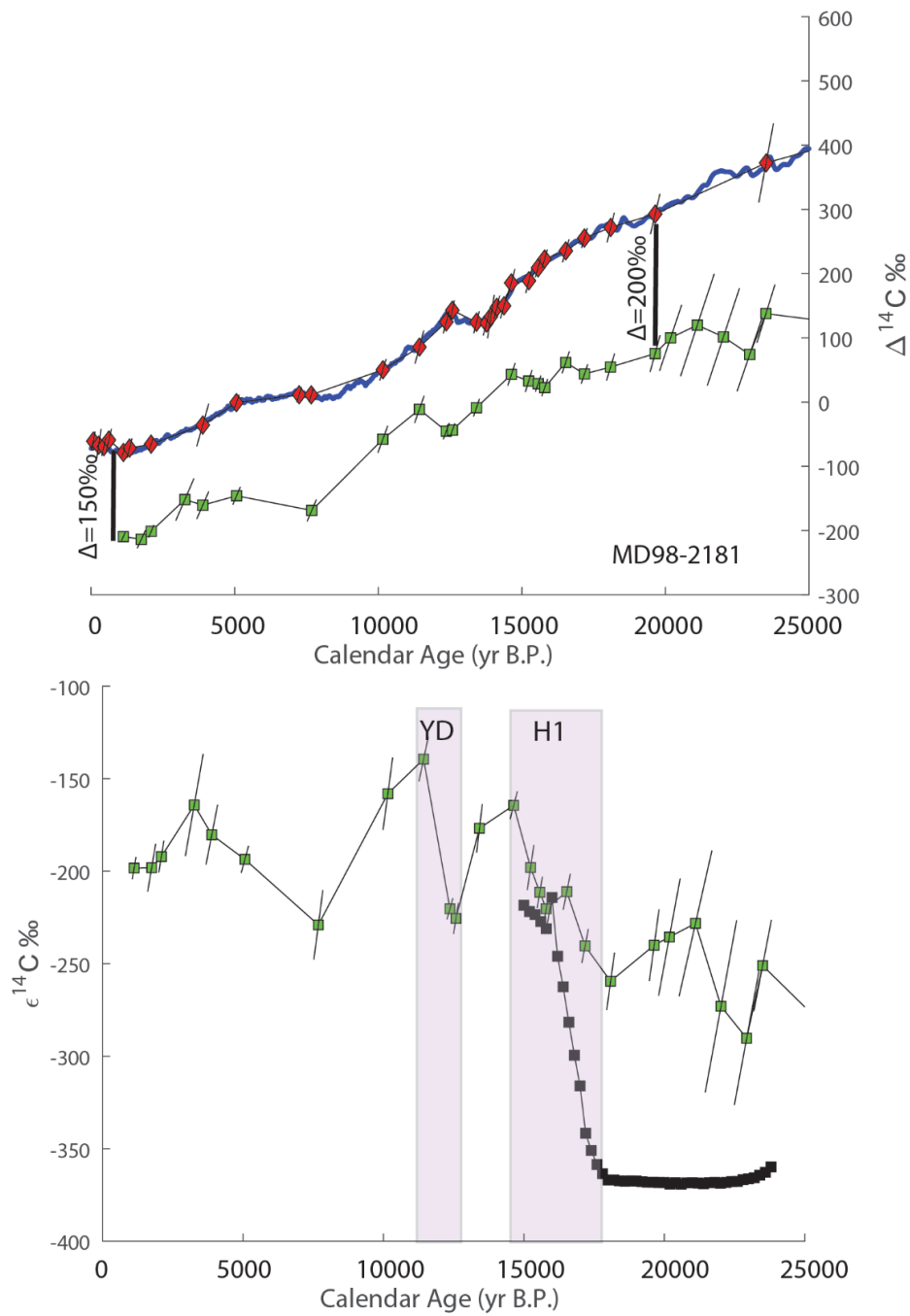


493

494 Supplemental Figure S1. GLODAP transect of  $\delta^{13}\text{C}_{\text{DIC}}$  (upper panel)  $\Delta^{14}\text{C}$  (middle panel)  
 495 through the Pacific. The location and depth of the MD98-2181 site is marked with a red X.

496





497

498 Supplemental Figure S2. Upper panel planktic  $\Delta^{14}\text{C}$  (red) and benthic  $\Delta^{14}\text{C}$  (green) with the  
 499 Mar20  $\Delta^{14}\text{C}$  record (blue). The quivers represent the combined age (horizontal) and radiometric  
 500 (vertical) uncertainties ( $1\sigma$ ). Lower panel shows MD98-2181 benthic  $\epsilon^{14}\text{C}$  (green) and the values  
 501 from the LOVECLIM simulation of Menviel et al. (2018) (black). The shaded intervals mark the  
 502 increases during the H1 and YD.

503